JACS Au
AN OPEN ACCESS JOURNAL OF THE AMERICAN CHEMICAL SOCIETY



pubs.acs.org/jacsau
Article

# Design and Evaluation of Pyridinyl Sulfonyl Piperazine LpxH Inhibitors with Potent Antibiotic Activity Against Enterobacterales

Amanda F. Ennis,[⊥] C. Skyler Cochrane,[⊥] Patrick A. Dome,[⊥] Pyeonghwa Jeong, Jincheng Yu, Hyejin Lee, Carly S. Williams, Yang Ha, Weitao Yang, Pei Zhou,* and Jiyong Hong*

Cite This: *JACS Au* 2024, 4, 4383−4393



**ABSTRACT:** Enterobacterales, a large order of Gram-negative bacteria, including *Escherichia coli* and *Klebsiella pneumoniae*, are major causes of urinary tract and gastrointestinal infections, pneumonia, and other diseases in healthcare settings and communities. ESBL-producing Enterobacterales and carbapenem-resistant Enterobacterales can break down commonly used antibiotics, with some strains being resistant to all available antibiotics. This public health threat necessitates the development of novel antibiotics, ideally targeting new pathways in these bacteria. Gram-negative bacteria possess an outer membrane enriched with lipid A, a saccharolipid that serves as the membrane anchor of lipopolysaccharides and the active component of the bacterial endotoxin, causing septic shock. The biosynthesis of lipid A is crucial for the viability of Gram-negative bacteria, and as an essential enzyme in this process, LpxH has emerged as a promising target for developing novel antibiotics against multidrug-resistant Gram-negative pathogens. Here, we report the development of pyridinyl sulfonyl piperazine LpxH inhibitors. Among them, *ortho*-substituted pyridinyl compounds significantly boost LpxH inhibition and antibiotic activity over the original phenyl series. Structural and QM/MM analyses reveal that these improved activities are primarily due to the enhanced interaction between F141 of the LpxH insertion lid and the pyridinyl group. Incorporation of the *N*-methyl-*N*-phenyl-methanesulfonamide moiety into the pyridinyl sulfonyl piperazine backbone results in JH-LPH-106 and JH-LPH-107, both of which exhibit potent antibiotic activity against wild-type Enterobacterales such as *K. pneumoniae* and *E. coli*. JH-LPH-107 exhibits a low rate of spontaneous resistance and a high safety window *in vitro*, rendering it an excellent lead for further clinical development.

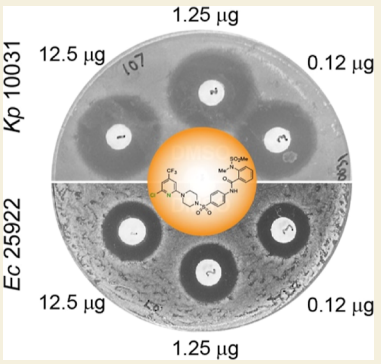


**KEYWORDS:** *antibiotics, Gram-negative bacteria, Enterobacterales, lipid A, LpxH, pyridinyl sulfonyl piperazine, N-methyl-N-phenyl-methanesulfonamide*

## INTRODUCTION

Enterobacterales, a significant order within Gram-negative bacteria, are responsible for a wide range of infections, such as urinary tract and gastrointestinal infections, pneumonia, meningitis, and sepsis. A major concern regarding Enterobacterales is the alarming rise of antibiotic resistance within this group. These bacteria exhibit a remarkable ability to develop resistance to multiple antibiotics through various mechanisms, including the production of $\beta$-lactamases, efflux pumps, and alterations in the bacterial cell wall.[1] This resistance significantly undermines the effectiveness of many commonly used antibiotics, resulting in prolonged illnesses, increased healthcare costs, and higher mortality rates. Particularly worrisome is the rise of extensively drug-resistant (XDR) and pan-drug-resistant (PDR) strains of Enterobacterales, such as extended-spectrum $\beta$-lactamase (ESBL)-producing Enterobacterales and carbapenem-resistant Enterobacterales (CREs). Infections caused by these strains are virtually untreatable with currently available antibiotics, prompting the CDC and WHO to classify these bacteria as serious and urgent threats.[2,3] Driven by the emergence of antibiotic-resistant strains and the limited efficacy of existing treatment options, there is an urgent need for new antibiotics against Enterobacterales.

Unlike Gram-positive bacteria, which have a single cell membrane, Gram-negative bacteria, such as Enterobacterales, have an additional outer membrane that serves as a protective shield against antibiotic penetration (Figure 1A). This outer membrane contains complex structures, such as lipopolysaccharides (LPS), that play essential roles in maintaining the bacterial structure, integrity, and interactions with the environment and human hosts. Serving as the hydrophobic anchor of LPS, lipid A and its constitutive biosynthesis are required for bacterial viability and fitness in the human host.[4−6]

Received: August 11, 2024
Revised: October 6, 2024
Accepted: October 30, 2024
Published: November 11, 2024





https://doi.org/10.1021/jacsau.4c00731
*JACS Au* 2024, 4, 4383−4393

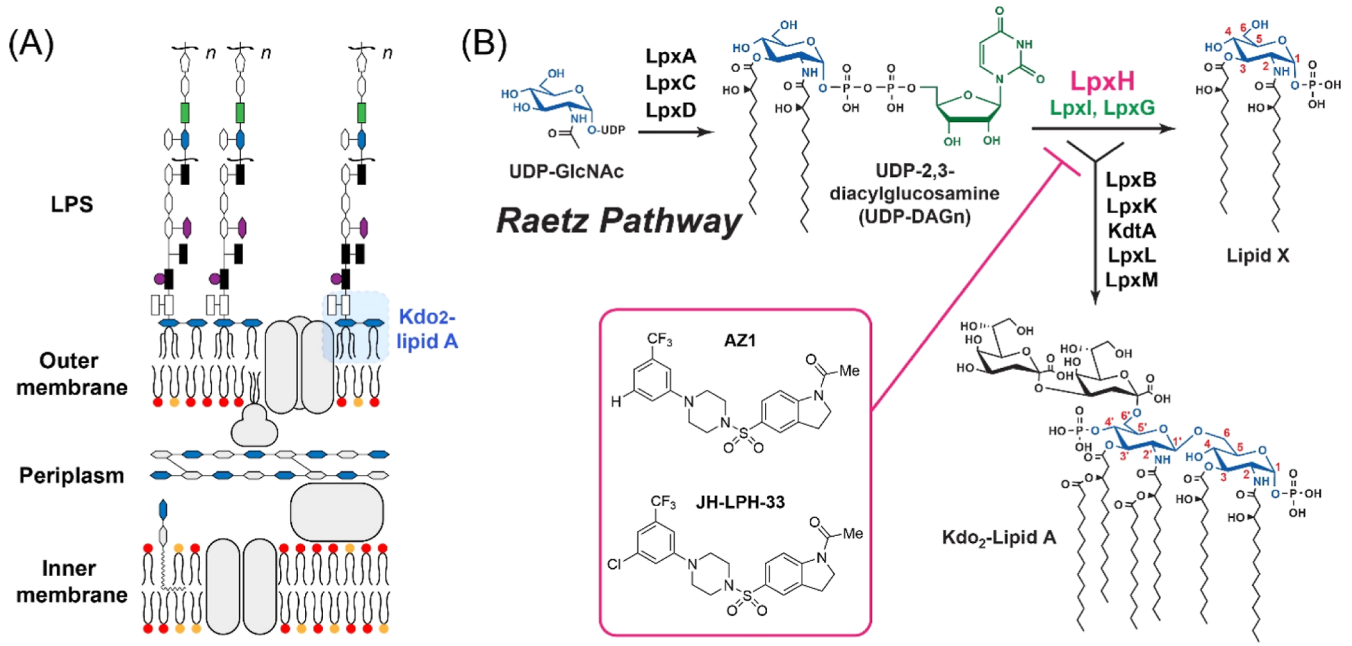


**Figure 1.** Lipid A biosynthesis in *E. coli*. (A) Schematic illustration of the *E. coli* cell envelope. (B) Raetz pathway of lipid A biosynthesis in *E. coli*. The inhibition of LpxH by the previously reported compounds AZ1 and JH-LPH-33 is indicated. Adapted from ref 19. Copyright 2021 American Chemical Society.

Lipid A biosynthesis, which is most thoroughly characterized in *Escherichia coli*—a prototypical bacterium of the Enterobacterales, involves nine enzymes in the Raetz pathway (Figure 1B).[4] The fourth step—and the first membrane-associated reaction in lipid A biosynthesis—the cleavage of the pyrophosphate group of UDP-DAGn to form lipid X—is carried out by one of three functional orthologs: LpxH in $\beta$- and $\gamma$-proteobacteria,[7] LpxI in $\alpha$-proteobacteria,[8] and LpxG in Chlamydiae.[9] Among these three enzymes, LpxH is most widespread, functioning in ∼70% of Gram-negative bacteria, including all clinically important Enterobacterales, such as *K. pneumoniae*, *E. coli*, and others. Following the hydrolysis reaction, five additional enzymes are required to generate $Kdo_2$-lipid A, which is sufficient to maintain bacterial viability in most Gram-negative organisms.

Since LpxH activity is required for the biosynthesis of lipid A and the integrity and functionality of the outer membrane, disruption of LpxH activity can significantly impact bacterial viability, virulence, and antibiotic resistance. Indeed, inhibition or genetic depletion of LpxH leads to toxic membrane accumulation of lipid A intermediates (i.e., the LpxH substrate UDP-DAGn) and distortion of the inner membrane,[10,11] resulting in an independent mechanism of bacterial killing in addition to the disruption of lipid A biosynthesis. Consistent with this notion, *Acinetobacter baumanii* can survive the loss of lipid A through null mutations in genes encoding early-stage lipid A enzymes (*lpxA*, *lpxC*, or *lpxD*). However, deletion of *lpxH* alone is lethal due to the toxic accumulation of the LpxH substrate.[12] Additionally, resistance mutations to LpxC inhibitors are most commonly found in the *fabZ* gene,[13,14] resulting in compromised fatty acid biosynthesis that rebalances reduced lipid A biosynthesis.[14] In contrast, resistance mutations to LpxH inhibitors, as shown in both literature[11] and our results below, occur almost exclusively in *lpxH* and not in *fabZ*. This further supports the idea that the toxic accumulation of the lipid A intermediate, UDP-DAGn (substrate of LpxH), cannot be mitigated by reducing fatty acid biosynthesis. These observations collectively underscore the unique therapeutic potential of novel antibiotics targeting LpxH in Gram-negative bacteria.

Understanding the structure and function of LpxH is critical to harnessing its therapeutic potential and has been of great interest in the field of antibacterial drug discovery. Research efforts focused on elucidating the structure and biochemical mechanisms of LpxH have provided valuable insights into its function and potential as a drug target.[15−17] To explore LpxH as a new antibiotic target against multidrug-resistant Gram-negative pathogens, we embarked on the development of LpxH inhibitors derived from AZ1 (Figure 1B), a sulfonyl piperazine inhibitor of LpxH identified through a high-throughput phenotypic screen by AstraZeneca.[11] To probe the molecular details of its interaction with LpxH, we crystallized *K. pneumoniae* LpxH in complex with AZ1 at 2.3 Å.[18] Unexpectedly, our NMR study revealed that there were two distinct conformations of LpxH-bound AZ1. Exploiting this ligand-dynamics information, we designed a more potent LpxH inhibitor, JH-LPH-33 (Figure 1B). Our crystal structure analysis of JH-LPH-33 in complex with *K. pneumoniae* LpxH confirmed our predicted binding mode, with the chloro group filling in the hydrophobic pocket occupied by the terminal methyl group of the 2 *N*-linked acyl chain shared by the substrate UDP-DAGn and product lipid X. Excitingly, JH-LPH-33 inhibited LpxH significantly more potently than AZ1. Building on these successes, herein we describe our effort toward the design, synthesis, and evaluation of a class of new pyridinyl sulfonyl piperazine LpxH inhibitors with outstanding antibiotic activity against wild-type Enterobacterales, such as *K. pneumoniae* and *E. coli*.


https://doi.org/10.1021/jacsau.4c00731
JACS Au 2024, 4, 4383−4393

## RESULTS AND DISCUSSION

### Synthesis and Characterization of Pyridine and Other Heteroaromatic Analogs of AZ1

**Synthesis.** After extensive exploration of the structural modification of the indoline part of AZ1,[18−22] we embarked on the modification of the trifluoromethyl-substituted phenyl tail part to further investigate the chemical space around AZ1. Toward this goal, we synthesized AZ1 derivatives with the trifluoromethylphenyl ring replaced with similarly substituted heteroaromatic rings such as pyridine, thiazole, or thiadiazole. The synthesis of these heteroaromatic analogs was accomplished following the procedures we have established for AZ1 (Scheme 1). Pd-mediated coupling of commercially available aryl bromides (**1a−e**) and *tert*-butyl piperazine-1-carboxylate (**2**) provided the Boc-protected *N*-pyridinyl and *N*-thiazolyl piperazines **3a−e** (Scheme 1A). Boc deprotection of **3a−e** by TFA followed by coupling of the resulting piperazines with commercially available 1-acetylindoline-5-sulfonyl chloride (**4**) proceeded smoothly to afford the desired pyridine and thiazole analogs JH-LPH-86, 89, 88, 90, and 85 (**5a−e**). Coupling of the commercially available 2-(piperazin-1-yl)-5-(trifluoromethyl)-1,3,4-thiadiazole (**6**) to **4** afforded the desired dithiazole analog JH-LPH-87 (**5f**), albeit in low yield (15%) (Scheme 1B). In a similar manner, the pyrimidine analogue JH-LPH-93 (**5g**) was prepared starting from 2-bromo-4-(trifluoromethyl)-pyrimidine (**1g**) (Scheme 1C).

**Scheme 1. Synthesis of Pyridine and Other Heteroaromatic Analogs of AZ1**

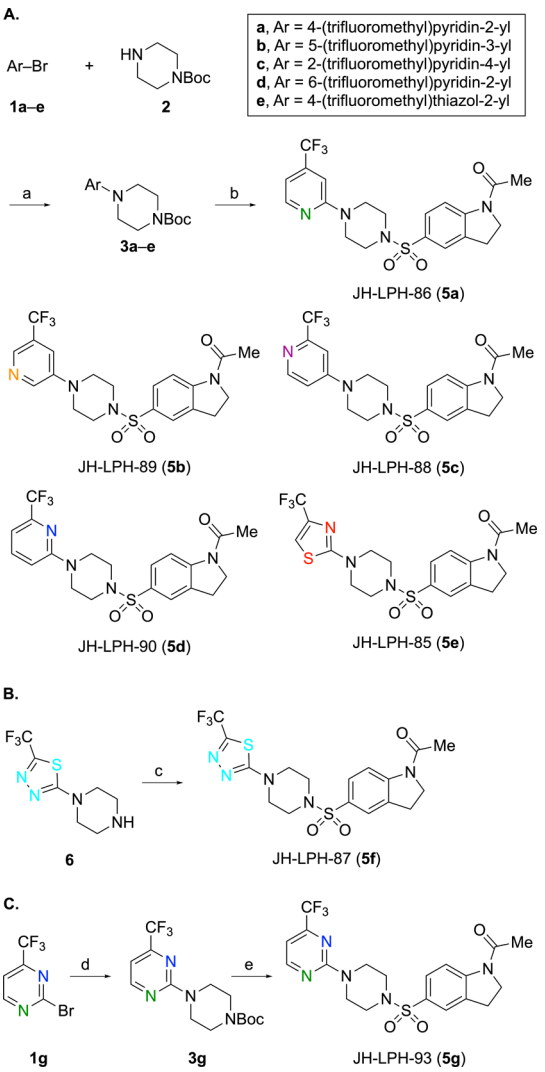


[a]$Pd_2(dba)_3$ (5 mol %), JohnPhos (10 mol %), NaO*t*-Bu, toluene, reflux, 15−18 h, **3a**: 57%, **3b**: 96%, **3c**: 80%, **3d**: 79%, **3e**: 69%. [b](i) TFA, $CH_2Cl_2$, 25 °C, 2 h; (ii) 1-acetylindoline-5-sulfonyl chloride (**4**), $Et_3N$, 1,4-dioxane, 60 °C, 3 h; 25 °C, 14−15 h, **5a**: 68%, **5b**: 10%, **5c**: 40%, **5d**: 14%, **5e**: 40% over two steps. [c]**4**, $Et_3N$, 1,4-dioxane, 60 °C, 3 h; 25 °C, 14 h, 15%. [d]**2**, $Pd_2(dba)_3$ (5 mol %), JohnPhos (10 mol %), NaO*t*-Bu, toluene, reflux, 15 h, 53%. [e](i) TFA, $CH_2Cl_2$, 25 °C, 2 h; (ii) **4**, $Et_3N$, 1,4-dioxane, 60 °C, 3 h; 25 °C, 14 h, 7% over two steps.

**Characterization.** The activities of the derivatives of the LpxH inhibitor, AZ1, with its trifluoromethyl-substituted phenyl ring replaced with similarly substituted heteroaromatic rings, were evaluated in our enzyme-coupled LpxH activity assay (Figures 2A and S1).[20] While AZ1 derivatives containing substitutions with five-membered heteroaromatic rings (JH-LPH-85 and JH-LPH-87) were generally less active than AZ1, we found that compounds with the pyridine nitrogen at different locations showed a distinct structure−activity relationship (SAR). Pyridine rings containing nitrogen at the *para*-position (JH-LPH-88) or *meta*-position (JH-LPH-89) to the piperazine ring had $IC_{50}$ values of 3182 nM and 2464 nM, respectively, reducing the potency of AZ1 ($IC_{50}$ = 360 nM) by ∼7−9 folds. In contrast, pyridine rings containing the nitrogen atom at the *ortho*-positions to the piperazine ring (JH-LPH-86 and JH-LPH-90; Figure 2A) dramatically enhanced the potency of LpxH inhibition over AZ1, reducing the $IC_{50}$ value of AZ1 from 360 to 85 nM for JH-LPH-86 and 112 nM for JH-LPH-90, corresponding to a 3.2- to 4.2-fold reduction of the $IC_{50}$ values.

The binding modes of JH-LPH-86 and JH-LPH-90 were determined by X-ray crystallography (statistics shown in Table S1). Both compounds exhibited binding modes that aligned closely with AZ1 in the crystal structure (Figure S2). Due to the lack of an obvious structural explanation for the observed SAR, we applied the symmetry-adapted perturbation theory (SAPT)[23,24] to investigate the noncovalent $\pi-\pi$ stacking between F141 of LpxH and the phenyl ring in AZ1 and the pyridine ring of JH-LPH-86 and JH-LPH-90. Aromatic rings are important moieties for biological interactions and protein−drug interactions. As $\pi-\pi$ (both stacking and T-shape), anion-$\pi$, and cation-$\pi$ are the main interaction types described in the literature,[25] we expected the noncovalent $\pi-\pi$ stacking between the side chain of F141 of LpxH and the aromatic rings in AZ1, JH-LPH-86, and JH-LPH-90 to be a key contributor to the binding free energy. Computational results from SAPT2 + 3 (Table S2) revealed that JH-LPH-86/90 have lower total interaction free energies compared to AZ1, with the most significant difference (∼1 kcal/mol) from the repulsive exchange term between the phenyl ring in AZ1 and the pyridine rings in JH-LPH-86/90 toward F141 of LpxH, while the differences among other energy components is lower than 0.5 kcal/mol. With one C atom in the phenyl ring replaced by the N atom in the pyridine ring, the repulsive interaction between JH-LPH-86/90 and F141 of LpxH is weaker than that between AZ1 and F141 of LpxH. With all the components (electrostatics, exchange, induction, and dispersion) combined, the total interaction energy between JH-LPH-86/90 and LpxH is ∼0.3 kcal/mol lower than that between AZ1 and LpxH, supporting the experimental observation of the stronger LpxH


https://doi.org/10.1021/jacsau.4c00731
JACS Au 2024, 4, 4383−4393

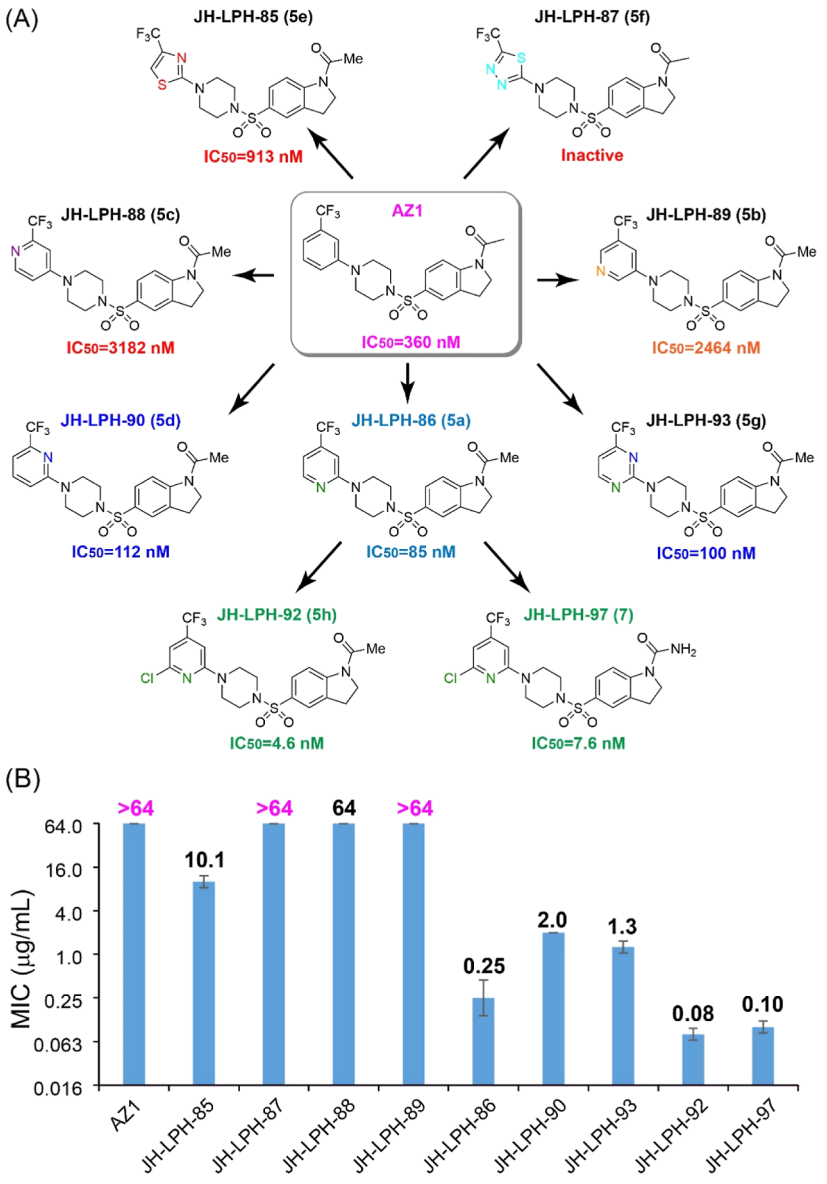


**Figure 2.** SAR of LpxH inhibitors. (A) Chemical structures and $IC_{50}$ values of LpxH inhibitors. (B) Antibiotic activities against *K. pneumoniae* 10031.

binding of JH-LPH-86/90 than AZ1. Since SAPT calculations are highly sensitive to the starting conformations, a similar analysis for the weaker JH-LPH-88 and JH-LPH-89 could not be reliably conducted due to the lack of structural information on their binding poses.

Encouraged by the significant enhancement of LpxH inhibition by the two pyridine analogs, we asked whether the enhanced potency of the *ortho*-nitrogen substituted pyridine compounds JH-LPH-86 and JH-LPH-90 could be combined. Therefore, we designed and synthesized a new analogue by converting the pyridine ring to the pyrimidine ring (Scheme 1C). Surprisingly, we found that the pyrimidine ring analog (JH-LPH-93) did not show further potency enhancement. Instead, it displayed weaker inhibition than that of JH-LPH-86 and had an $IC_{50}$ value of 100 nM (Figure 2A).

## Chloro-Substitution of the Trifluoromethyl Pyridine Compound Further Enhances Potency

**Synthesis.** We previously reported that the trifluoromethyl substituted LpxH inhibitor AZ1 adopted two distinct conformations when bound to LpxH, with the two conformations correlated with a ring flipping event.[18] This led to the design of JH-LPH-33 with an additional chloro-substitution at the *meta*-position. JH-LPH-33 dramatically improved the potency of AZ1. To determine whether a similar chloro incorporation is beneficial, we combined the chloro-substitution at the *meta*-position in JH-LPH-33 (Figure 1) with the pyridine group in JH-LPH-86 and designed the 2-chloro-4-triflouromethyl pyridine analogue JH-LPH-92 (**5h**, Scheme 2). Starting from commercially available 2-bromo-6-chloro-4-(trifluoromethyl)pyridine (**1h**), Pd-mediated coupling of **1h** with *tert*-butyl piperazine-1-carboxylate (**2**) provided the Boc-protected *N*-pyridinyl piperazine **3h**. Boc deprotection of **3h** by TFA followed by coupling of the resulting piperazine with 1-acetylindoline-5-sulfonyl chloride (**4**) in the presence of $Et_3N$ proceeded smoothly to afford the desired 2-chloro-4-triflouromethyl-substituted pyridine analog JH-LPH-92. Acetyl deprotection of JH-LPH-92 under acidic conditions, followed by treatment with CDI and $NH_4OH$, completed the synthesis


https://doi.org/10.1021/jacsau.4c00731
JACS Au 2024, 4, 4383−4393

**Scheme 2. Synthesis of 2-Chloro-4-triflouromethyl Pyridine Analogs**

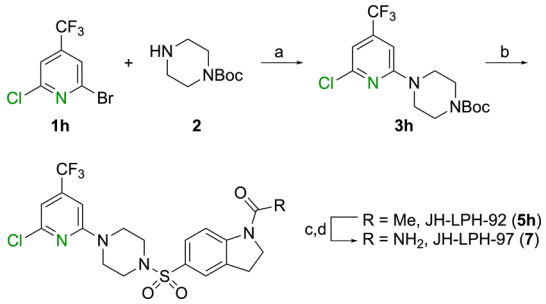


[a]$Pd_2(dba)_3$ (5 mol %), JohnPhos (10 mol %), NaO*t*-Bu, toluene, reflux, 15 h, 56%. [b](i) TFA, $CH_2Cl_2$, 25 °C, 2 h; (ii) 1-acetylindoline-5-sulfonyl chloride (**4**), $Et_3N$, 1,4-dioxane, 60 °C, 3 h; 25 °C, 14 h, 83% over two steps. [c]*c*-HCl, EtOH, reflux, 2 h. [d](i) CDI, DMAP, MeCN, 90 °C, 24 h; (ii) $NH_4OH$, 90 °C, 16 h, 45% over two steps.

of the corresponding urea derivative JH-LPH-97 (**7**). The urea derivative JH-LPH-97 was expected to have enhanced aqueous solubility compared to JH-LPH-92.

**Characterization.** Similar to our previous report that the doubly substituted phenyl ring with a trifluoromethyl and a chloro group in JH-LPH-33 significantly enhances the potency of AZ1, we found that the 2-chloro-4-trifluoromethyl substituted derivatives (JH-LPH-92 and JH-LPH-97) of the pyridine compound JH-LPH-86 further reduced the $IC_{50}$ value from 85 to 4.6 nM (JH-LPH-92) and 7.6 nM (JH-LPH-97), corresponding to 11- to 18-fold further enhancement of the LpxH inhibition (Figures 2A and S1). Our analysis of the crystal structure of JH-LPH-92 bound to *K. pneumoniae* LpxH (Table S1 and Figure S3) revealed a binding mode similar to that of the previously reported phenyl compound, JH-LPH-33, corroborating that the pyridine substitution of the phenyl group is the main contributing factor to the enhancement in potency.

Accompanying the dramatic improvement in the potency of these compounds for LpxH inhibition over AZ1, there is a corresponding enhancement of antibiotic activity (Figure 2B). Even though the parent compound AZ1 and its disubstituted derivative JH-LPH-33 displayed weak to modest antibiotic activity when tested against *K. pneumoniae* 10031, with MIC values of >64 and 1.6 μg/mL, respectively, the *ortho*-substituted pyridine compounds JH-LPH-86, JH-LPH-92, and JH-LPH-97 dramatically reduced the MIC values to 0.25, 0.08, and 0.10 μg/mL, respectively, corresponding to ∼16- to 25-fold reduction of the MIC values for the pyridine compounds in comparison with their parent compounds containing a phenyl ring (JH-LPH-86 vs AZ1; JH-LPH-92 and JH-LPH-97 vs JH-LPH-33).

With the significant enhancement of *in vitro* LpxH inhibition by the pyridine group, some of these pyridine analogs, e.g., JH-LPH-97, started to display measurable antibiotic activity against WT *E. coli* 25922 (MIC = 13 μg/mL, Table 1). Encouraged by this success, we embarked on the search for additional structural motifs that would further improve the potency of the LpxH inhibitors.

## Incorporation of the *N*-Methyl-*N*-Phenyl-Methanesulfonamide Group

In parallel with our lead optimization effort, researchers at Uppsala University recently reported a screening effort, leading to the discovery of a new LpxH inhibitor, JEDI-852, from the PubChem Library (PubChem AID 573), which occupies the active site of LpxH.[26] Recognizing the overlapping structural moiety between JEDI-852 and AZ1, the Uppsala team was able to fuse the two compounds and create novel LpxH inhibitors with MICs in the range of 0.5−1 μg/mL against *K. pneumoniae* and 1−2 μg/mL against *E. coli* ATCC 25922.[26] As the Uppsala compounds were based on the pyrimidine series, which showed weaker activity than the pyridine series in our analysis, we investigated the effect of the *N*-methyl-*N*-phenyl-methanesulfonamide group on our pyridinyl sulfonyl piperazine LpxH inhibitors by incorporating the *N*-methyl-*N*-phenyl-methanesulfonamide group into our LpxH aniline and indoline cores and prepared two pyridine-methylsulfonamide hybrid analogs (JH-LPH-106 and JH-LPH-107; Figure 3A).

**Synthesis.** The syntheses of JH-LPH-106 (**10**) and JH-LPH-107 (**12**) were achieved, as illustrated in Scheme 3. Compound **8**, which is the intermediate in the synthesis of JH-LPH-97 (**7**, Scheme 2), was coupled to 2-(*N*-methylmethylsulfonamido)benzoic acid **9** (see the Supporting Information for the synthesis of **9**) in the presence of $SOCl_2$ and $Et_3N$ to afford JH-LPH-106 (**10**). For the synthesis of JH-LPH-107 (**12**), compound **3h** was converted to aniline **11** via Boc deprotection, coupling with 4-acetamidobenzenesulfonyl chloride and Ac deprotection. Final coupling of **11** with **9** completed the synthesis of JH-LPH-107 (**12**) in a 70% yield.

**Biological Activity of JH-LPH-106 and 107.** Incorporation of the *N*-methyl-*N*-phenyl-methanesulfonamide group into our pyridine compound scaffold yielded JH-LPH-106 and JH-LPH-107 with an impressive enhancement of the potency. The indoline compound JH-LPH-106 inhibited *K. pneumoniae* LpxH with an $IC_{50}$ value of 0.044 nM and *E. coli* LpxH with an $IC_{50}$ value of 0.058 nM, whereas the aniline compound JH-LPH-107 inhibited both *K. pneumoniae* and *E. coli* LpxH with an $IC_{50}$ value of 0.13 nM (Figures 3B and S1 and Table 1). Considering that JH-LPH-92, the parent compound of JH-LPH-106, has an $IC_{50}$ value of 4.6 nM against *K. pneumoniae* LpxH, the incorporation of the *N*-methyl-*N*-phenyl-methanesulfonamide group resulted in a potency enhancement of ∼100-fold. Our crystal structural analysis of JH-LPH-106 and JH-LPH-107 in complex with *K. pneumoniae* LpxH shows that the *N*-methyl-*N*-phenyl-methanesulfonamide group forms perpendicular $\pi-\pi$ stacking with the side chains of Y125 and F128 and hydrogen bonds with R80 of the enzyme, both of which would contribute to a significant enhancement of the binding affinity (Table S1 and Figure S4). These compounds are considerably more potent than the Uppsala lead compounds, EBL-3647 and EBL-3599, which were reported to inhibit *E. coli* LpxH with $IC_{50}$ values of 2.2 and 3.5 nM, respectively.[26] Since these assays were done using different substrate concentrations, we converted the $IC_{50}$ values to $K_i$ values based on the modality of competitive inhibition, as reported previously.[18] The pyridine-derived LpxH inhibitors JH-LPH-106 and JH-LPH-107 inhibited *E. coli* and *K. pneumoniae* LpxH enzymes with $K_i$ values from 0.02−0.05 nM, whereas the Uppsala compounds EBL-3647 and EBL-3599 had much weaker $K_i$ values from 1.7−2.6 nM.

The superior potency of pyridine compounds JH-LPH-106 and JH-LPH-107 against *E. coli* and *K. pneumoniae* LpxH is nicely reflected by the dramatic enhancement of the antibiotic activities of these compounds, which is evident by the large sizes of the killing zones of JH-LPH-107 against wild-type *K. pneumoniae* 10031 and *E. coli* 25922 in the bacterial disc


https://doi.org/10.1021/jacsau.4c00731
JACS Au 2024, 4, 4383−4393

**Table 1. LpxH Inhibitors and Characterization**[a]

| Compounds | Structure | $IC_{50}$ (nM)* | *K. pneumoniae* 10031 MIC (μg/mL) | *E. coli* 25922 MIC (μg/mL) |
|---|---|---|---|---|
| AZ1[#] | 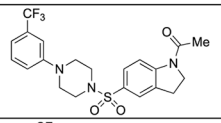 | 360 | >64 | Inactive |
| JH-LPH-33[#] | 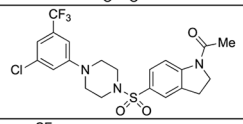 | 26 | 1.6 | Inactive |
| JH-LPH-86 **(5a)** | 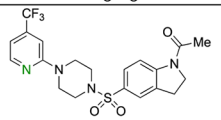 | 85 | 0.25 | >64 |
| JH-LPH-89 **(5b)** | 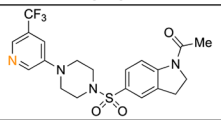 | 2,464 | >64 | ND |
| JH-LPH-88 **(5c)** | 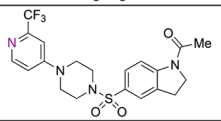 | 3,182 | 64 | ND |
| JH-LPH-90 **(5d)** | 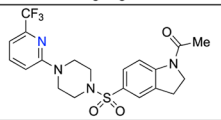 | 112 | 2.0 | ND |
| JH-LPH-85 **(5e)** | 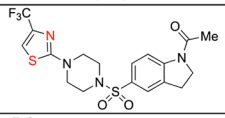 | 913 | 10.1 | ND |
| JH-LPH-87 **(5f)** | 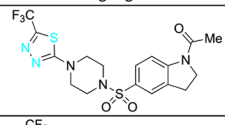 | >100,000 | >64 | ND |
| JH-LPH-93 **(5g)** | 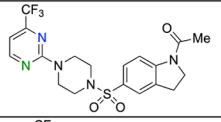 | 100 | 1.3 | ND |
| JH-LPH-92 **(5h)** | 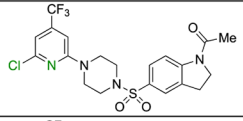 | 4.6 | 0.08 | >64 |
| JH-LPH-97 **(7)** | 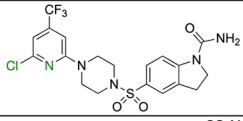 | 7.6 | 0.10 | 13 |
| JH-LPH-106 **(10)** | 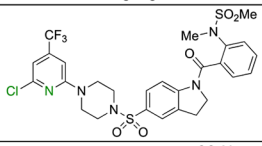 | 0.044 (0.058) | 0.04 | 0.63 |
| JH-LPH-107 **(12)** | 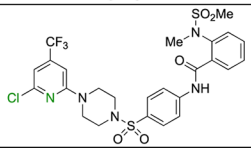 | 0.13 (0.13) | 0.04 | 0.31 |

[a]*: Assayed against *K. pneumoniae* LpxH except for values in parentheses, which were assayed against *E. coli* LpxH. [#]: Value from Cho *et al.* PNAS 2020. ND: Not determined.

diffusion assays (Figure 3D). When measured using the liquid broth microdilution assay, JH-LPH-106 had MIC values of 0.63 μg/mL against WT *E. coli* 25922 and 0.04 μg/mL against *K. pneumoniae* 10031, whereas JH-LPH-107 had MIC values of



https://doi.org/10.1021/jacsau.4c00731
JACS Au 2024, 4, 4383−4393

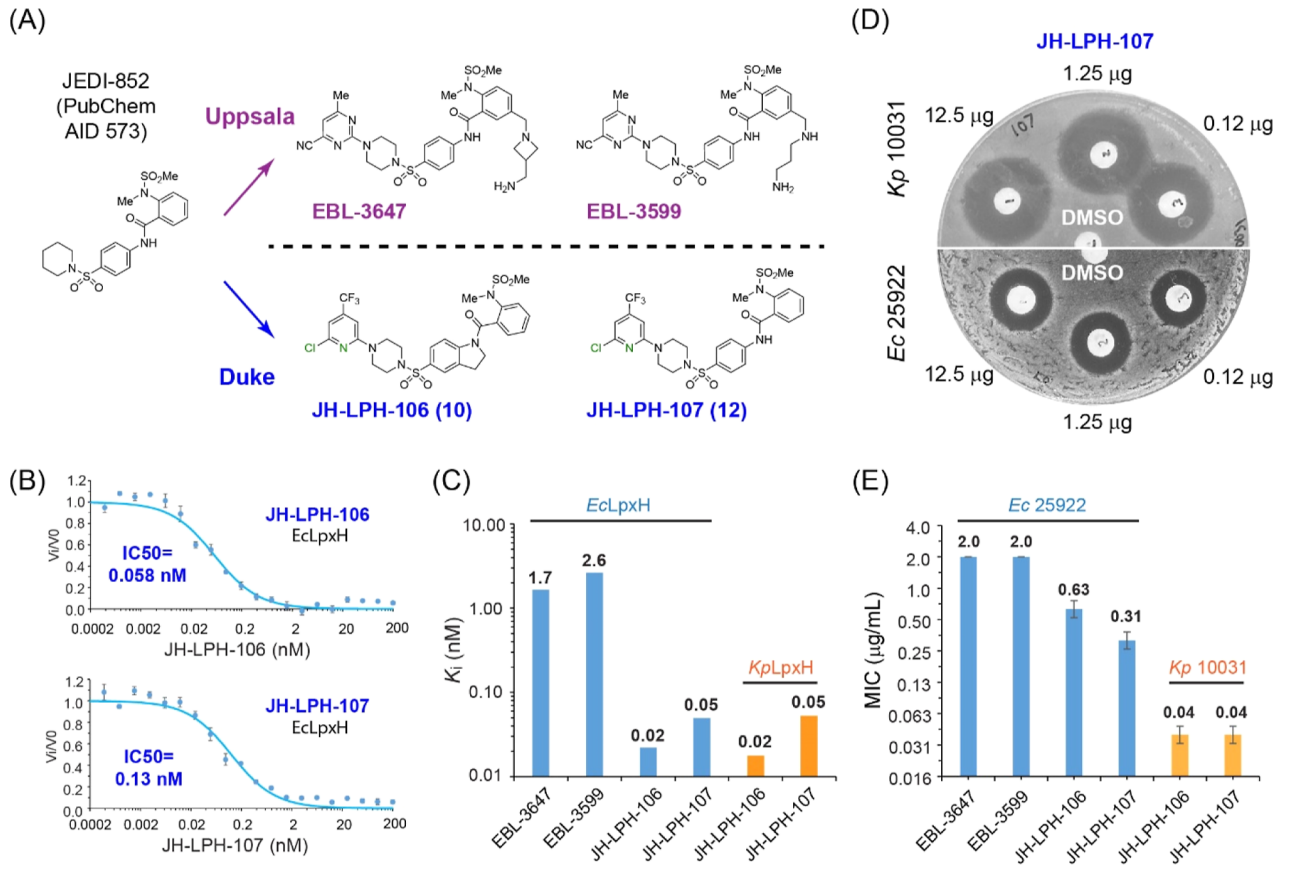


**Figure 3.** Incorporation of JEDI-852, from the PubChem Library (PubChem AID 573), enhances the potency of LpxH inhibitors. (A) Uppsala and Duke LpxH inhibitors. (B) Dose-dependent LpxH inhibition curves by JH-LPH-106 (top panel) and JH-LPH-107 (lower panel). (C) $K_i$ values of LpxH inhibitors assayed against *E. coli* LpxH (*Ec*LpxH) and *K. pneumoniae* LpxH (*Kp*LpxH) (D) Antibiotic activity of JH-LPH-107 against wild-type *K. pneumoniae* 10031 (*Kp* 10031) and *E. coli* 25922 (*Ec* 25922) in the bacterial disc diffusion assay. (E) MICs of Uppsala and Duke Compounds. Values of Uppsala compounds (EBL-3647 and EBL-3599) are reported by Huseby et al.[26]

**Scheme 3. Synthesis of Pyridine-Methanesulfonamide Hybrid Analogs (JH-LPH-106 and JH-LPH-107)**

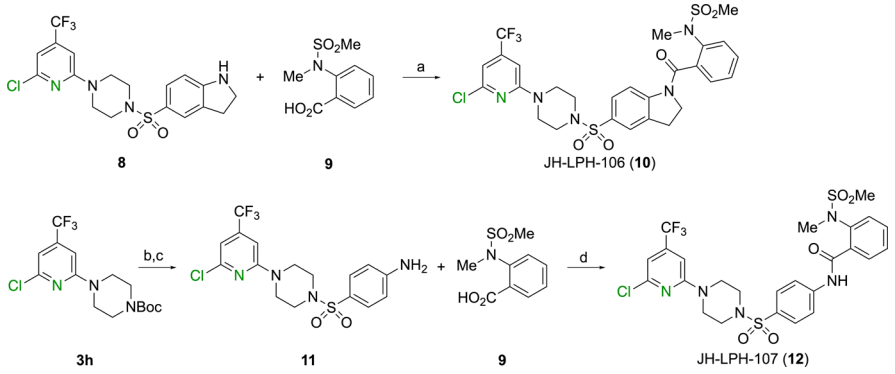


[a](i) $SOCl_2$, reflux, 18 h; (ii) $Et_3N$, 0 to 25 °C, 4 h, 68%. [b](i) TFA, $CH_2Cl_2$, 25 °C, 2 h; (ii) 4-acetamidobenzenesulfonyl chloride, $Et_3N$, 1,4-dioxane, 60 °C, 3 h; 30 °C, 15 h, 51% over two steps. [c]c-HCl, EtOH, reflux, 2 h, 51%. [d](i) $SOCl_2$, reflux, 18 h; (ii) $Et_3N$, 0 to 25 °C, 4 h, 70%.

0.31 μg/mL against *E. coli* 25922 and 0.04 μg/mL against *K. pneumoniae* 10031 (Table 1 and Figure 3E). Both compounds significantly outperformed the Uppsala lead compounds EBL-3647 and EBL-3599 with reported MIC values of 2.0 μg/mL against *E. coli* 25922 by 3- to 6.5-folds.

## Time-Kill Kinetics, Spontaneous Resistance Mutation, and *In Vitro* Safety

JH-LPH-107 appears to be a bactericidal antibiotic against the *K. pneumoniae* 10031, reducing bacterial viability by > 1000-fold within 6 h and preventing regrowth up to 24 h at or above the MIC (Figure S5). The rate of spontaneous resistance mutations to the LpxH inhibitor, JH-LPH-107, was evaluated in *K. pneumoniae* 10031 and *E. coli* 25922, resulting in a frequency range of $2.0-2.5 \times 10^{-9}$ at 4× MIC and $0.9-1.4 \times 10^{-9}$ at 8× MIC (Table 2). The isolated resistant mutations were exclusively present in the target *lpxH* gene, with the most prevalent mutations mapped to F141 (F141L in *K. pneumoniae lpxH* and F141L, F141C, and F141S in *E. coli lpxH*); additional mutations F128C and R80C in *E. coli* were also


https://doi.org/10.1021/jacsau.4c00731
JACS Au 2024, 4, 4383−4393

Table 2. Spontaneous Resistance Mutation to JH-LPH-107

| Strain | Rate of spontaneous resistance mutations | | Mutations |
|---|---|---|---|
| | @4× MIC | @8× MIC | |
| *K. pneumoniae* 10031 | $2.0 \times 10^{-9}$ | $9.1 \times 10^{-10}$ | F141L: TTC to CTC (n=2)<br>F141L: TTC to TTG (n=2) |
| *E. coli* 25922 | $2.5 \times 10^{-9}$ | $1.4 \times 10^{-9}$ | F141L: TTC to CTC (n=4)<br>F141C: TTC to TGC (n=4)<br>F141S: TTC to TCC (n=1)<br>R80H: CGT to CAT (n=2)<br>F128C: TTT to TGT (n=1) |

observed (Table 2). These mutations correspond to LpxH interactions with the pyridine group (F141 and F128) and *N*-methyl-*N*-phenyl-methanesulfonamide (R80), respectively. Of note, this result is in sharp contrast with the spontaneous resistance mutations isolated for inhibitors of LpxC, the second enzyme of the lipid A biosynthetic pathway. Most resistance mutations to LpxC inhibitors did not reside within the *lpxC* target gene but instead occurred in the *fabZ* gene in the fatty acid biosynthetic pathway.[13,14] This rebalancing of phospholipid and lipid A biosynthesis counteracted the effect of LpxC inhibition.[14] As the inhibition of LpxH leads to toxic membrane accumulation of lipid A intermediates (i.e., the LpxH substrate UDP-DAGn) and distortion of the inner membrane,[10,11] resulting in an independent mechanism of bacterial killing in addition to disruption of lipid A biosynthesis, inhibition of LpxH cannot be overcome by mutations in the *fabZ* gene.

JH-LPH-107 appeared to be safe *in vitro*: when evaluated against HEK293 or HepG2 cells, it did not cause any significant cytotoxicity at 100 $\mu$M (63 $\mu$g/mL) (Figure S6AB). Considering its MICs of 0.31 $\mu$g/mL and 0.04 $\mu$g/mL against *E. coli* 25922 and *K. pneumoniae* 10031, respectively, JH-LPH-107 has a large safety index of >100-fold, rendering it a promising lead for further development into clinical therapeutics.

## CONCLUSIONS

We have developed a new series of sulfonyl piperazine LpxH inhibitors with enhanced *in vitro* activity and MIC values. Incorporation of a pyridine ring, but not a pyrimidine ring, into the AZ1 structure dramatically enhances the LpxH inhibition by analogs. We showed that the pyridine ring can also be incorporated in the disubstituted JH-LPH-33 scaffold and additionally merged with JEDI-852 from the PubChem Library (PubChem AID 573), discovered by the Uppsala team, to yield superior antibiotics against wild-type Enterobacterales, with the lead compound JH-LPH-107 displaying MICs of 0.31 and 0.04 $\mu$g/mL against *E. coli* 25922 and *K. pneumoniae* 10031. JH-LPH-107 has low spontaneous resistant mutation rates of $2.0-2.5 \times 10^{-9}$ at 4× MIC and $0.9-1.4 \times 10^{-9}$ at 8× MIC and has no significant cytotoxicity against HEK293 or HepG2 cells at >100-fold of the MIC. These significant advancements have highlighted LpxH as a viable antibiotic target, particularly against multidrug-resistant Enterobacterales, such as the extended-spectrum $\beta$-lactamase (ESBL)-producing Enterobacterales and CREs, that pose serious threats to public health.

## EXPERIMENTAL SECTION

### Synthesis of LpxH Inhibitors

Details of the synthesis and characterization of LpxH inhibitors are presented in the Supporting Information.

### Computational Details

Theoretical calculations were performed to investigate the noncovalent interactions between F141 of LpxH and the aromatic rings of AZ1 and JH-LPH-86/90 with the SAPT[23] at the SAPT2 + 3 level[27] using the Psi4 package.[28] All calculations were performed with the aug-cc-pVDZ basis set[29,30] using the truncated crystal structures. To reduce the computational cost, both LpxH and the ligands were truncated. For LpxH, the phenyl group involved in the $\pi-\pi$ stacking was kept, and the rest of the molecule was replaced with a methyl group. For AZ1 and JH-LPH-86/90, the molecules were truncated at the N−S bond. Geometries used for the calculations are documented in the Supporting Information.

### MIC Assay

The MIC assay was conducted following protocols adapted from the National Committee for Clinical Laboratory Standard's broth microdilution methods,[31] utilizing 96-well plates as previously outlined.[18,21,22] Briefly, bacterial cultures grown overnight were diluted to an $OD_{600}$ of 0.006 in cation-adjusted Mueller−Hinton medium containing 7% DMSO, then incubated at 37 °C for 22 h with varying inhibitor concentrations. After overnight incubation, each well received 10 $\mu$L of 3-(4,5-dimethylthiazol-2-yl)-2,5-diphenyltetrazolium bromide (MTT, 5 mg/mL) for 3 h. Subsequently, the culture was solubilized with 2-propanol, and the results were determined by measuring the difference in UV absorbance at 570 and 690 nm. MIC values were defined as the lowest compound concentration inhibiting bacterial growth, with UV readings within 4-fold of those from the wells containing no bacteria.

### Enzymatic Assay for LpxH Inhibition

The LpxE-coupled LpxH activity assay[20] was performed following established procedures using the GB1-*K. pneumoniae* LpxH-$His_{10}$ fusion protein and GB1-*E. coli* LpxH-$His_{10}$ fusion protein.[18,21,22] Two reaction mixtures were prepared: Mixture 1 consisted of 20 mM Tris−HCl (pH 8.0), 0.5 mg/mL BSA, 0.02% Triton X-100, 1 mM $MnCl_2$, 1 mM DTT, 10% DMSO, and 200 $\mu$M substrate (UDP-DAGn), while Mixture 2 contained the same buffer components but replaced the substrate with LpxH (20 ng/mL and 10 ng/mL for *K. pneumoniae* LpxH and *E. coli* LpxH, respectively) and 2× inhibitor. In the cases of LPH-106 and LPH-107, 10-fold less LpxH was used, and the overall time course of the assay was expanded. After preincubation of the mixtures at 37 °C for 10 min, the reaction was initiated by combining an equal volume of Mixture 2 with Mixture 1 at 37 °C. The final reaction mixture comprised 100 $\mu$M substrate, 10 ng/mL *K. pneumoniae* LpxH (1 ng/mL *K. pneumoniae* LpxH or 0.5 ng/mL *E. coli* LpxH for LPH-106 and LPH-107), and 1× inhibitor. At designated time points, 20 $\mu$L aliquots of the reaction mixture were quenched by the addition to wells containing 5 mM EDTA in a 96-well half a rea



https://doi.org/10.1021/jacsau.4c00731
JACS Au 2024, 4, 4383−4393

plate to halt the LpxH reaction. *Aquifex aeolicus* LpxE (5 $\mu$g/mL) was then added, followed by a 30 min incubation at 37 °C before quenching the LpxE reaction with formic acid (final concentration: 3.75 M). The malachite green reagent (Sigma-Aldrich, catalog MAK307) was diluted 5-fold into the solutions, incubated for 30 min at room temperature, and absorbance at 620 nm was measured. All measurements were conducted in triplicates, and the standard error was calculated. The $IC_{50}$ values were extracted from the fitting of the dose−response curve of $\frac{v_i}{v_0} = \frac{1}{1+\frac{[I]}{IC_{50}}}$. Under the mode of competitive inhibition, $IC_{50} = K_I^*(1 + [S]/K_M)$, with the substrate $K_M$ = 68.1 $\mu$M and 61.7 $\mu$M for LpxH enzymes from *K. pneumoniae* and *E. coli*, respectively.[7,18]

## Cloning and Purification of *Kp*LpxH

Cloning and purification of *Kp*LpxH for crystallography studies were conducted following previously documented procedures.[18,21,22] In summary, *Kp*LpxH was inserted into a modified pET21b vector (Novagen/Millipore Sigma), resulting in the LpxH fusion protein featuring a C-terminal TEV protease site (ENLYFQGS) followed by a $His_{10}$ tag. BL21 STAR (DE3) *E. coli* cells (Thermo Fisher Scientific) transformed with the vector were cultured in LB medium at 37 °C until reaching an $OD_{600}$ of 0.5 and then induced with 1 mM IPTG for an additional 3 h at 37 °C before being harvested by centrifugation. The protein purification process was conducted at 4 °C. Cell pellets obtained from 8 L of induced culture were suspended and lysed in 120 mL of lysis buffer, consisting of 50 mM phosphate-citrate, 20 mM MES (pH 6.0), 600 mM NaCl, 10% sucrose, 5 mM 2-mercaptoethanol, 10 mM imidazole, and 0.1% Triton X-100, using a French press. Centrifugation at 40,000×*g* for 40 min removed cell debris, and the resulting supernatant was applied to a column containing 20 mL of HisPur $Ni^{2+}$-NTA resin (Thermo Fisher Scientific), pre-equilibrated with 100 mL of lysis buffer. Following extensive washing with purification buffer composed of 20 mM phosphate-citrate, 20 mM MES (pH 6.0), 300 mM NaCl, 5% glycerol, 5 mM 2-mercaptoethanol, and 40 mM imidazole, LpxH was eluted from the column through a stepwise increase in imidazole concentration from 40 to 500 mM in the purification buffer. Subsequent concentration for further purification was achieved through size-exclusion chromatography (Superdex 200; GE Healthcare Life Sciences) in FPLC buffer containing 20 mM MES (pH 6.0), 600 mM NaCl, 1 mM DTT, and 5% glycerol.

## Co-crystallization of *Kp*LpxH with Various Inhibitors

The FPLC peak fractions containing *K. pneumoniae* LpxH were pooled and concentrated for crystallization. Compounds JH-LPH-86, JH-LPH-90, JH-LPH-92, JH-LPH-106, and JH-LPH-107 were added to the LpxH solution in two steps to minimize the DMSO concentration while still ensuring more than a 1:1 concentration of LpxH to compounds. First, a 1:1 molar ratio of each compound was added to the FPLC fraction prior to concentrating them to the final concentration. Then, another 1:1 ratio of the compounds was added after concentrating the FPLC fractions immediately before setting up the crystal trays. Protein crystals were grown using the sitting-drop vapor diffusion method at 20 °C. Each drop was prepared by mixing 1 $\mu$L of the protein solution with 1 $\mu$L of the reservoir solution.

The final drop solution for JH-LPH-86 contained 1 mg/mL LpxH, 0.14 mM JH-LPH-86, 10 mM MES (pH 6.0), 100 mM NaCl, 0.5 mM DTT, 2.5% glycerol, 0.8% DMSO, 0.05 M sodium acetate pH 5.0, and 18% v/v PEG 400.

The final drop solution for JH-LPH-90 contained 1.2 mg/mL of LpxH, 0.16 mM JH-LPH-90, 10 mM MES (pH 6.0), 100 mM NaCl, 0.5 mM DTT, 2.5% glycerol, 0.8% DMSO, 0.05 M HEPES pH 7.0, and 18% w/v PEG 400.

The final drop solution for JH-LPH-92 contained 1.25 mg/mL of LpxH, 0.16 mM JH-LPH-92, 10 mM MES (pH 6.0), 100 mM NaCl, 0.5 mM DTT, 2.5% glycerol, 0.8% DMSO, 0.05 M sodium acetate pH 5.0, and 17% w/v PEG 400.

The final drop solution for JH-LPH-106 contained 1.1 mg/mL LpxH, 0.15 mM JH-LPH-106, 10 mM MES (pH 6.0), 100 mM NaCl, 0.5 mM DTT, 2.5% glycerol, 0.8% DMSO, 0.05 M HEPES pH 6.5, and 18% w/v PEG 400.

The final drop solution for JH-LPH-107 contained 0.91 mg/mL LpxH, 0.1 mM JH-LPH-107, 10 mM MES (pH 6.0), 100 mM NaCl, 0.5 mM DTT, 2.5% glycerol, 0.8% DMSO, 0.05 M sodium acetate pH 4.5, and 16% v/v PEG 400.

Diffraction quality protein crystals were harvested after 1−2 weeks and soaked for 5−15 min with a cryoprotectant composed of mother liquor diluted 40% additionally containing 30% glycerol, 100 $\mu$M $MnCl_2$, 1% DMSO, and 20 $\mu$M of the respective compound.

## Time-Kill Kinetics

For time-kill kinetics, individual colonies of *K. pneumoniae* 10031 were selected and grown to $OD_{600}$ = 1.0 prior to 1000× dilution into 10 mL of LB media containing 1% DMSO and 0×, 0.5×, 1×, 2×, 4×, 8×, or 16× MIC JH-LPH-107. The cultures were then grown at 37 °C for 24 h. Aliquots were taken from each sample at various time points between 1 and 24 h and diluted in LB media in serial 1:10 dilutions. 5 mL droplets of each sample and its serial dilutions were spotted on LB agar plates and incubated at 37 °C for 24 h. The CFU/mL was calculated from the lowest dilution that maintained countable individual colonies.

## Spontaneous Resistance Development

To assess the rate of spontaneous resistance mutations, target strains, *E. coli* 25922 and *K. pneumoniae* 10031, were first grown on antibiotic-free LB agar plates. Individual colonies were selected (5−6/strain) and grown to $OD_{600}$ = 1 before being resuspended in 1/10th of their original volume. Subsequently, 0.1 mL of each concentrated culture was taken to determine the initial CFU/mL, and 0.2 mL of each culture was plated on LB agar plates containing either 4 or 8× MIC JH-LPH-107. After 48 h of incubation at 37 °C, all resulting colonies were passaged a second time on a fresh 8× MIC JH-LPH-107 plate and allowed to grow for an additional 48 h. At this time, the resulting colonies were counted and sent for sequencing to determine the resistance mutations occurring. The frequency of resistance is calculated as the ratio of the growth found on the JH-LPH-107 supplemented agar plate to the density of the initial inoculum.

## *In Vitro* Cytotoxicity Assay

To determine the toxicity of JH-LPH-107, a CellTiter-Glo 2.0 cell viability assay was utilized, which measures the number of metabolically active cells based on the ATP content. In this assay, HEK-293 or HepG2 cells were plated in a 96-well plate format with 1000 cells per well and given 24 h to adhere. JH-LPH-107 was then added by serial dilution from 100 to 0.39 $\mu$M, and HEK-293 or HepG2 cells were incubated for 24 h. The CellTiter-Glo 2.0 cell viability assay kit (Promega) was used according to the manufacturer's instructions, with the substrate being diluted at a 1:1 ratio. A total of 100 $\mu$L of this mixture was added to the cells and incubated for 5 min at room temperature before luminescence values. Luminescence values were normalized to the DMSO control. The assay was performed in triplicate.

# ■ ASSOCIATED CONTENT

## Supporting Information

The Supporting Information is available free of charge at https://pubs.acs.org/doi/10.1021/jacsau.4c00731.

Detailed descriptions of all synthetic procedures, $^1$H NMR data, X-ray data collection and refinement statistics, SAPT calculations, dose−response curves of inhibitors tested against *K. pneumoniae* LpxH, comparison of the crystal structures of JH-LPH-86, JH-LPH-90, and AZ1, overlay of the crystal structure of the *K. pneumoniae* LpxH/JH-LPH-92 complex with that of the *K. pneumoniae* LpxH/JH-LPH-33 complex, expanded interaction network surrounding the *N*-methyl-*N*-phenyl-methanesulfonamide moiety of JH-LPH-106



https://doi.org/10.1021/jacsau.4c00731
JACS Au 2024, 4, 4383−4393

and JH-LPH-107, time-kill kinetics of JH-LPH-107 against *K. pneumoniae* 10031, and cytotoxicity of JH-LPH-107 (PDF)

## AUTHOR INFORMATION


### Corresponding Authors

**Pei Zhou** − *Department of Chemistry, Duke University, Durham, North Carolina 27708, United States; Department of Biochemistry, Duke University School of Medicine, Durham, North Carolina 27710, United States;* orcid.org/0000-0002-7823-3416; Email: peizhou@biochem.duke.edu

**Jiyong Hong** − *Department of Chemistry, Duke University, Durham, North Carolina 27708, United States; Department of Pharmacology and Cancer Biology, Duke University School of Medicine, Durham, North Carolina 27710, United States;* orcid.org/0000-0002-5253-0949; Email: jiyong.hong@duke.edu

### Authors

**Amanda F. Ennis** − *Department of Chemistry, Duke University, Durham, North Carolina 27708, United States*

**C. Skyler Cochrane** − *Department of Chemistry, Duke University, Durham, North Carolina 27708, United States; Department of Biochemistry, Duke University School of Medicine, Durham, North Carolina 27710, United States*

**Patrick A. Dome** − *Department of Chemistry, Duke University, Durham, North Carolina 27708, United States*

**Pyeonghwa Jeong** − *Department of Chemistry, Duke University, Durham, North Carolina 27708, United States*

**Jincheng Yu** − *Department of Chemistry, Duke University, Durham, North Carolina 27708, United States;* orcid.org/0000-0001-8487-5565

**Hyejin Lee** − *Department of Chemistry, Duke University, Durham, North Carolina 27708, United States*

**Carly S. Williams** − *Department of Biochemistry, Duke University School of Medicine, Durham, North Carolina 27710, United States*

**Yang Ha** − *Berkeley Center for Structural Biology, Molecular Biophysics and Integrated Bioimaging, Lawrence Berkeley National Laboratory, Berkeley, California 94720, United States;* orcid.org/0000-0001-5684-8420

**Weitao Yang** − *Department of Chemistry, Duke University, Durham, North Carolina 27708, United States;* orcid.org/0000-0001-5576-2828

Complete contact information is available at: https://pubs.acs.org/10.1021/jacsau.4c00731


### Author Contributions

[⊥]A.F.E., C.S.C., and P.A.D. contributed equally to this work. CRediT: **Amanda F Ennis** investigation, writing - review & editing; **C Skyler Cochrane** formal analysis, investigation, visualization, writing - review & editing; **Patrick A Dome** investigation, writing - review & editing; **Pyeonghwa Jeong** investigation, writing - review & editing; **Jincheng Yu** formal analysis, investigation, writing - review & editing; **Hyejin Lee** investigation, writing - review & editing; **Carly S Williams** formal analysis, investigation, visualization, writing - review & editing; **Yang Ha** investigation, visualization, writing - review & editing; **Weitao Yang** supervision, validation, writing - review & editing; **Pei Zhou** conceptualization, formal analysis, funding acquisition, project administration, supervision, validation, visualization, writing - original draft, writing - review & editing; **Jiyong Hong** conceptualization, funding acquisition, project administration, supervision, validation, visualization, writing - original draft, writing - review & editing.

### Notes

The authors declare the following competing financial interest(s): J.H. and P.Z. are inventors of patents covering the designed LpxH inhibitors.

## ACKNOWLEDGMENTS

This work was supported in part by the grants from the National Institute of Allergy and Infectious Diseases (NIH R01AI139216), the National Institute of General Medical Sciences (NIH R01GM115355), and the Gilhuly Accelerator Fund. W.Y. and J.Y. acknowledge support from the National Institute of Health (NIH R01GM061870). A.F.E. was supported by the NIGMS Pharmacological Sciences Training Grant (NIH T32GM133352). X-ray diffraction data for the LpxH/JH-LPH-86 complex were collected at the Northeastern Collaborative Access Team beamlines, which are funded by the National Institute of General Medical Sciences from the National Institutes of Health (P30 GM124165). The Eiger 16M detector on the 24-ID-E beamline is funded by a NIH-ORIP HEI grant (S10OD021527). This research used resources of the Advanced Photon Source, a U.S. Department of Energy (DOE) Office of Science User Facility operated for the DOE Office of Science by Argonne National Laboratory under contract no. DE-AC02-06CH11357. The authors would like to thank Diamond Light Source for beamtime (proposal mx442), and the staff of beamlines I02, I03, and I24 for assistance with crystal testing and data collection of the LpxH/JH-LPH-90 complex. Crystal data of LpxH in complexes with JH-LPH-92, JH-LPH-106, and JH-LPH-107 were collected at the Advanced Light Source (ALS) beamlines 5.0.2 and 5.0.3 operated by the Berkeley Center for Structural Biology (BCSB). BCSB is supported by the Howard Hughes Medical Institute, Participating Research Team members, and the National Institutes of Health, National Institute of General Medical Sciences, ALS-ENABLE grant P30 GM124169. The Advanced Light Source is a Department of Energy Office of Science User Facility under Contract no. DE-AC02-05CH11231.

## REFERENCES

(1) Darby, E. M.; Trampari, E.; Siasat, P.; Gaya, M. S.; Alav, I.; Webber, M. A.; Blair, J. M. A. Molecular mechanisms of antibiotic resistance revisited. *Nat. Rev. Microbiol.* **2023**, *21*, 280−295.

(2) CDC. *Antibiotic Resistance Threats in the United States, 2019*; U.S., Department of Health and Human Services, CDC: Atlanta, GA, 2019.

(3) *WHO Bacterial Priority Pathogens List, 2024: bacterial pathogens of public health importance to guide research, development and strategies to prevent and control antimicrobial resistance*; World Health Organization: Geneva, 2024, pp 10−14.

(4) Raetz, C. R. H.; Whitfield, C. Lipopolysaccharide endotoxins. *Annu. Rev. Biochem.* **2002**, *71*, 635−700.

(5) Zhou, P.; Barb, A. Mechanism and inhibition of LpxC: an essential zinc-dependent deacetylase of bacterial lipid A synthesis. *Curr. Pharm. Biotechnol.* **2008**, *9*, 9−15.

(6) Zhou, P.; Zhao, J. Structure, inhibition, and regulation of essential lipid A enzymes. *Biochim. Biophys. Acta, Mol. Cell Biol. Lipids* **2017**, *1862*, 1424−1438.

(7) Babinski, K. J.; Ribeiro, A. A.; Raetz, C. R. The *Escherichia coli* gene encoding the UDP-2,3-diacylglucosamine pyrophosphatase of lipid A biosynthesis. *J. Biol. Chem.* **2002**, *277*, 25937−25946.
(8) Metzger, L. E. t.; Raetz, C. R. An alternative route for UDP-diacylglucosamine hydrolysis in bacterial lipid A biosynthesis. *Biochem.* **2010**, *49*, 6715−6726.
(9) Young, H. E.; Zhao, J.; Barker, J. R.; Guan, Z.; Valdivia, R. H.; Zhou, P. Discovery of the elusive UDP-Diacylglucosamine hydrolase in the lipid A biosynthetic pathway in *Chlamydia trachomatis*. *mBio* **2016**, *7*, No. e00090.
(10) Babinski, K. J.; Kanjilal, S. J.; Raetz, C. R. Accumulation of the lipid A precursor UDP-2,3-diacylglucosamine in an *Escherichia coli* mutant lacking the lpxH gene. *J. Biol. Chem.* **2002**, *277*, 25947−25956.
(11) Nayar, A. S.; Dougherty, T. J.; Ferguson, K. E.; Granger, B. A.; McWilliams, L.; Stacey, C.; Leach, L. J.; Narita, S.; Tokuda, H.; Miller, A. A.; Brown, D. G.; McLeod, S. M. Novel antibacterial targets and compounds revealed by a high-throughput cell wall reporter assay. *J. Bacteriol.* **2015**, *197*, 1726−1734.
(12) Richie, D. L.; Takeoka, K. T.; Bojkovic, J.; Metzger, L. E. t.; Rath, C. M.; Sawyer, W. S.; Wei, J. R.; Dean, C. R. Toxic accumulation of LPS pathway intermediates underlies the requirement of LpxH for growth of *Acinetobacter baumannii* ATCC 19606. *PLoS One* **2016**, *11*, No. e0160918.
(13) Clements, J. M.; Coignard, F.; Johnson, I.; Chandler, S.; Palan, S.; Waller, A.; Wijkmans, J.; Hunter, M. G. Antibacterial activities and characterization of novel inhibitors of LpxC. *Antimicrob. Agents Chemother.* **2002**, *46*, 1793−1799.
(14) Zeng, D.; Zhao, J.; Chung, H. S.; Guan, Z.; Raetz, C. R.; Zhou, P. Mutants resistant to LpxC inhibitors by rebalancing cellular homeostasis. *J. Biol. Chem.* **2013**, *288*, 5475−5486.
(15) Cho, J.; Lee, C. J.; Zhao, J.; Young, H. E.; Zhou, P. Structure of the essential *Haemophilus influenzae* UDP-diacylglucosamine pyrophosphohydrolase LpxH in lipid A biosynthesis. *Nat. Microbiol.* **2016**, *1*, 16154.
(16) Okada, C.; Wakabayashi, H.; Kobayashi, M.; Shinoda, A.; Tanaka, I.; Yao, M. Crystal structures of the UDP-diacylglucosamine pyrophosphohydrase LpxH from *Pseudomonas aeruginosa*. *Sci. Rep.* **2016**, *6*, 32822.
(17) Bohl, H. O.; Ieong, P.; Lee, J. K.; Lee, T.; Kankanala, J.; Shi, K.; Demir, O.; Kurahashi, K.; Amaro, R. E.; Wang, Z.; Aihara, H. The substrate-binding cap of the UDP-diacylglucosamine pyrophosphatase LpxH is highly flexible, enabling facile substrate binding and product release. *J. Biol. Chem.* **2018**, *293*, 7969−7981.
(18) Cho, J.; Lee, M.; Cochrane, C. S.; Webster, C. G.; Fenton, B. A.; Zhao, J.; Hong, J.; Zhou, P. Structural basis of the UDP-diacylglucosamine pyrophosphohydrolase LpxH inhibition by sulfonyl piperazine antibiotics. *Proc. Natl. Acad. Sci. U.S.A.* **2020**, *117*, 4109−4116.
(19) Zhou, P.; Hong, J. Structure- and ligand-dynamics-based design of novel antibiotics targeting lipid A enzymes LpxC and LpxH in Gram-negative bacteria. *Acc. Chem. Res.* **2021**, *54*, 1623−1634.
(20) Lee, M.; Zhao, J.; Kwak, S. H.; Cho, J.; Lee, M.; Gillespie, R. A.; Kwon, D. Y.; Lee, H.; Park, H. J.; Wu, Q.; Zhou, P.; Hong, J. Structure-activity rlationship of sulfonyl piperazine LpxH inhibitors analyzed by an LpxE-coupled malachite green assay. *ACS Infect. Dis.* **2019**, *5*, 641−651.
(21) Kwak, S. H.; Cochrane, C. S.; Ennis, A. F.; Lim, W. Y.; Webster, C. G.; Cho, J.; Fenton, B. A.; Zhou, P.; Hong, J. Synthesis and evaluation of sulfonyl piperazine LpxH inhibitors. *Bioorg. Chem.* **2020**, *102*, 104055.
(22) Kwak, S. H.; Skyler Cochrane, C.; Cho, J.; Dome, P. A.; Ennis, A. F.; Kim, J. H.; Zhou, P.; Hong, J. Development of LpxH inhibitors chelating the active site dimanganese metal cluster of LpxH. *ChemMedChem* **2023**, *18*, No. e202300023.
(23) Jeziorski, B.; Moszynski, R.; Szalewicz, K. Perturbation theory approach to intermolecular potential energy surfaces of van der Waals complexes. *Chem. Rev.* **1994**, *94*, 1887−1930.
(24) Parker, T. M.; Burns, L. A.; Parrish, R. M.; Ryno, A. G.; Sherrill, C. D. Levels of symmetry adapted perturbation theory (SAPT). I. Efficiency and performance for interaction energies. *J. Chem. Phys.* **2014**, *140*, 094106.
(25) Salonen, L. M.; Ellermann, M.; Diederich, F. Aromatic rings in chemical and biological recognition: energetics and structures. *Angew. Chem., Int. Ed. Engl.* **2011**, *50*, 4808−4842.
(26) Huseby, D. L.; Cao, S.; Zamaratski, E.; Sooriyaarachchi, S.; Ahmad, S.; Bergfors, T.; Krasnova, L.; Pelss, J.; Ikaunieks, M.; Loza, E.; Katkevics, M.; Bobileva, O.; Cirule, H.; Gukalova, B.; Grinberga, S.; Backlund, M.; Simoff, I.; Leber, A. T.; Berruga-Fernández, T.; Antonov, D.; Konda, V. R.; Lindström, S.; Olanders, G.; Brandt, P.; Baranczewski, P.; Vingsbo Lundberg, C.; Liepinsh, E.; Suna, E.; Jones, T. A.; Mowbray, S. L.; Hughes, D.; Karlén, A. Antibiotic class with potent *in vivo* activity targeting lipopolysaccharide synthesis in Gram-negative bacteria. *Proc. Natl. Acad. Sci. U.S.A.* **2024**, *121*, No. e2317274121.
(27) Hohenstein, E. G.; Sherrill, C. D. Density fitting of intramonomer correlation effects in symmetry-adapted perturbation theory. *J. Chem. Phys.* **2010**, *133*, 014101.
(28) Smith, D. G. A.; Burns, L. A.; Simmonett, A. C.; Parrish, R. M.; Schieber, M. C.; Galvelis, R.; Kraus, P.; Kruse, H.; Di Remigio, R.; Alenaizan, A.; James, A. M.; Lehtola, S.; Misiewicz, J. P.; Scheurer, M.; Shaw, R. A.; Schriber, J. B.; Xie, Y.; Glick, Z. L.; Sirianni, D. A.; O'Brien, J. S.; Waldrop, J. M.; Kumar, A.; Hohenstein, E. G.; Pritchard, B. P.; Brooks, B. R.; Schaefer, H. F.; Sokolov, A. Y.; Patkowski, K.; DePrince, A. E.; Bozkaya, U.; King, R. A.; Evangelista, F. A.; Turney, J. M.; Crawford, T. D.; Sherrill, C. D. Psi4 1.4: Open-source software for high-throughput quantum chemistry. *J. Chem. Phys.* **2020**, *152*, 184108.
(29) Dunning, T. H. Gaussian basis sets for use in correlated molecular calculations. I. The atoms boron through neon and hydrogen. *J. Chem. Phys.* **1989**, *90*, 1007−1023.
(30) Woon, D. E.; Dunning, T. H. Gaussian basis sets for use in correlated molecular calculations. IV. Calculation of static electrical response properties. *J. Chem. Phys.* **1994**, *100*, 2975−2988.
(31) *Methods for Dilution Antimicrobial Susceptibility Tests for Bacteria that Grow Aerobically*; 11th ed; Clinical and Laboratory Standards Institute, 2018; CLSI standard M07.


https://doi.org/10.1021/jacsau.4c00731
*JACS Au* 2024, 4, 4383−4393